AD_____

Award Number: W81XWH-04-1-0249

TITLE: Improved Sensitivity and Specificity for Detection of Prostate Cancer

PRINCIPAL INVESTIGATOR: Rao P. Gullapalli, Ph.D.

CONTRACTING ORGANIZATION: University of Maryland Baltimore
Baltimore, MD 21201

REPORT DATE: April 2005

TYPE OF REPORT: Annual

PREPARED FOR: U.S. Army Medical Research and Materiel Command
Fort Detrick, Maryland 21702-5012

REPORT DOCUMENTATION PAGE

Form Approved
OMB No. 0704-0188

1. REPORT DATE *(DD-MM-YYYY)*	2. REPORT TYPE	3. DATES COVERED *(From - To)*
01-04-2005	Annual	1 Mar 2004 - 28 Feb 2005

4. TITLE AND SUBTITLE

Improved Sensitivity and Specificity for Detection of Prostate Cancer

5a. CONTRACT NUMBER

5b. GRANT NUMBER
W81XWH-04-1-0249

5c. PROGRAM ELEMENT NUMBER

6. AUTHOR(S)

Rao P. Gullapalli, Ph.D.

5d. PROJECT NUMBER

5e. TASK NUMBER

5f. WORK UNIT NUMBER

7. PERFORMING ORGANIZATION NAME(S) AND ADDRESS(ES)

University of Maryland
Baltimore
Baltimore, MD 21201

8. PERFORMING ORGANIZATION REPORT NUMBER

9. SPONSORING / MONITORING AGENCY NAME(S) AND ADDRESS(ES)
U.S. Army Medical Research and Materiel Command
Fort Detrick, Maryland 21702-5012

10. SPONSOR/MONITOR'S ACRONYM(S)

11. SPONSOR/MONITOR'S REPORT NUMBER(S)

12. DISTRIBUTION / AVAILABILITY STATEMENT
Approved for Public Release; Distribution Unlimited

13. SUPPLEMENTARY NOTES

14. ABSTRACT

Abstract is on page 4 of the report.

15. SUBJECT TERMS
Prostate, spectroscopy, MRI

16. SECURITY CLASSIFICATION OF:			17. LIMITATION OF ABSTRACT	18. NUMBER OF PAGES	19a. NAME OF RESPONSIBLE PERSON
a. REPORT	b. ABSTRACT	c. THIS PAGE			19b. TELEPHONE NUMBER *(include area code)*
U	U	U	UU	18	

Table of Contents

Abstract

The award was made on September 24, 2003 for which the Award/contract was received on Jan 22, 2004. The Internal Review Board approval was obtained from the University of Maryland, Baltimore on May 11, 2004. This information was provided to the Department of Defense. The approved IRB protocol was then submitted to the Army office of the Surgeon General's Human Subjects Review Board (HSRRB) in June of 2004. This review process is still ongoing. The latest communication that we received was on April 28, 2005 which asks for clarification of a couple of minor issues and to make the language easy in the consent form such that a person with an 8th standard education could understand. In essence our work on humans has not started. As the process of human subject research approval continues we have made some headway in optimizing our algorithms for deformation correction of the prostate as is required for Specific Aim 1.

As soon as the HSRRB approves the application, we will submit the modified protocol to the Internal Review Board of the University of Maryland, Baltimore for their approval upon whose approval we will commence the research on human subjects.

Improved Sensitivity and Specificity for Detection of Prostate

PC031042

HSRRB Log No. A-12577

Introduction

The goal of this proposal is to diagnose prostate cancer more effectively using various magnetic resonance imaging techniques available with the ultimate goal of providing information with high specificity for either treatment planning purposes or patient management. To achieve this goal we would like to address the following two specific aims.

Specific Aim 1: To estimate the efficacy of image morphing and fusion techniques required providing appropriate distortion corrections on prostate images obtained from an endorectal coil for a more accurate assessment of the correlation between MRI/MRSI and histopathology.

Specific Aim 2: The development of a tumor index based on individual MRI/MRSI characteristics through correlation with step-section histology for a more accurate determination of the tumor extent and aggressiveness.

Body

Overall Status of the Project:

We have made some headway in tackling Specific Aim 1 of this project and the details are given below. We have not yet started any human research as we are still awaiting the approval from Surgeon General's Human Subjects Review Board (HSRRB). We originally obtained IRB approval from our own institution. The IRB was approved in May of 2004. Following its approval we submitted the application to HSRRB and it has gone through two revisions so far. We think the approval process is in its final stages and we are waiting to hear from them any day now. Once the approval comes through we will have to submit the HSRRB approved changes to our local IRB for their approval. In our view human subject research is at least three months away and will realistically start around the first of September. Meanwhile we have made significant headway in tackling Specific Aim 1. We have now built a realistic prostate phantom which mimics the prostates tissue properties both physically and biochemically. We have test our distortion correction algorithms on this phantom and also on some pre-existing MRI data of human prostate. Soon we will be collecting images of a resected intact prostate that is available in our pathology department and performing whole mount cuts at 2mm sections and digitizing the cuts. Our goal is to reconstruct the digitized image into a three-dimensional prostate and co-register with the MR images of the intact prostate. These samples will enable us fine tune our technique before we actually start recruiting patients into this study. This exercise will be take place in the month of June and we hope to complete it by mid-July.

Brief Overview

MR spectroscopic information of the prostate is obtained by inserting an endorectal coil. The coils has an inflatable balloon that is typically inflated to about 100 cc in order to tightly couple with the prostate gland and avoid any involuntary motion of the gland during the imaging process. Such positioning of the coil allows one to obtain the maximum signal to noise achievable while imaging this gland. The insertion of coil physically distorts the prostate gland and MRI/MRSI is obtained with the prostate gland in this deformed state. However, when the prostate is removed during prostatectomy, the shape of the prostate is completely different from the position when MRI/MRSI was obtained (deformed state) and also when the endorectal coil was not inserted (normal state). For accurate correlation of histology with the MRI/MRSI it becomes essential that the resected prostate be registered to the prostate in its deformed state and also the normal state (when no coil was present). To accurately characterize the prostate from the imaging findings, it is necessary to obtain 3-dimensional data that encompasses the complete prostate in vivo and then register this image set with the three dimensional images obtained from the resected prostate prior to step-sectioning. Further, the thin sections from step-sectioning will need to be digitized and reconstructed as a whole prostate and registered to the in-vivo and ex-vivo images of the prostated. This will allow us to spatially correlate the imaging findings to that of the histopathology accurately. This is an exercise in morphing and registration, for which we have developed the tools and are in the process of validating. The tools that we have constructed in order to accomplish the goals include the construction of a 'realistic' prostate phantom and optimization of algorithms that perform elastic registration of deformed objects.

Appendix A shows the abstract that was accepted as a poster and published under the Proceedings of the Thirteenth International Society of Magnetic Resonance in Medicine conducted in Miami Beach. Appendix B shows the actual poster that was presented at this meeting.

Appendix C shows preliminary results obtained from a novel algorithm for elastic registration that uses strain minimization criteria both on simulated objects and on actual prostate images. As mentioned in our grant application we have already developed the deformation correction and registration algorithms that we will be using for the project. However, we continue to explore other algorithms that further optimize elastic registration of deformable objects. Appendix C shows one such approach that we have been working on lately.

Key Research Accomplishments

To date we have been able to do the following:

1. Build a prostate phantom for validating all registration and deformation correction algorithm.
2. Explore novels methods of elastic registration.
3. Implement all the tools necessary for the data analysis of the prostate imaging data.

Reportable Outcomes

We have not yet started our research work on humans. We anticipate this work to start about three months from the date of this report. Meanwhile we have presented our data on the prostate phantom at an international meeting and have been pursuing novel algorithms for elastic registration. We anticipate submitting works from both these projects to peer reviewed journals.

Conclusions

A major accomplishment for this project has been the development of the prostate phantom. The prostate phantom as designed serves as a useful training tool for physicians as they can practice prostate biopsy and ultrasound guided radioactive seed placement during brachytherapy. The

phantom can be used for quality control of spectroscopic scans. It also serves as a useful model to test registration algorithms for deformable objects. More importantly the phantom can be used to normalize prostate imaging data from different sites and also to normalize data imaging data obtained from different MR vendor's machines.

At the time of writing this report we are still awaiting the approval from HSRRB which appears to be in its final stages. Following their approval we will be submitting an amended application to our institutional IRB to be able to conduct human research. We hope to start this work in about three month's time.

APPENDIX A

Multi-Purpose Prostate Phantom

B. Zhang[1], R. P. Gullapalli[1]
[1]Diagnostic Radiology Department, University of Maryland, Baltimore, Baltimore, MD, United States

Introduction

Endorectal coil MR imaging of the prostate has become a standard methodology for diagnosis of prostate cancer. MRI of the prostate using the endorectal coil along with spectroscopic imaging have shown to improve the sensitivity and specificity of cancer detection [Kurhanewicz 2000]. However techniques such as MRSI still pose a major challenge in the successful execution of the exam. Given the nature of the exam and the unavailability of a suitable test bed before using the technique on humans exacerbates the problem. Further any information obtained from MRI regarding the prostate is in its deformed state since the endorectal coil deforms the prostate. For proper treatment planning such as brachytherapy, it becomes essential that this deformation is corrected before the information is used for either TRUS biopsy or ultrasound guided brachytherapy. Several deformation correction algorithms [Mizowaki T, 2002] exist, but lack a suitable phantom to check for the accuracy of the correction provided by these algorithms. We have constructed a first proto-type of such a phantom mainly for MRI use although it could be used by other modalities and here we provide some preliminary results from this work.

Materials and Methods

In constructing the prostate phantom the T1 and T2 values of the prostate was given primary consideration followed by the Young's modulus of the prostate tissue from previously reported studies [Kemper J, 2004, Hamhaber U, 2003]. The size of the prostate was an elliptical sphere of dimensions 52x41x35 mm^3 and was constructed using 0.5% agarose gels doped with 0.1mM Gd-DTPA. The biochemicals choline (10mM), creatine (30mM), citrate (100mM) and Lactate (35 mM) that are predominantly seen in prostate MRSI were also added. To mimic implanted seeds, we used sesame seeds that were randomly distributed within the prostate. Lard was used to mimic the periprostatic fat and formed the outer layer of the entire prostate. The phantom as shown in fig 1 allows for insertion of the endorectal coil or an ultrasound transducer through a 1.25 inch diameter hole and allows for the inflation of the balloon of the endorectal coil. The phantom was imaged on Philips Eclipse 1.5T system and spectra were obtained using a PRESS CSI sequence (TE/TR=130/1500ms) with frequency selective fat and water suppression.

Results

The T1 for the prostate, fat, and background material were 589, 148 and 1880ms respectively. The T2 values were 73, 53, and 90ms respectively. The Young's modulus of the prostate was about 3kPa and these values are consistent with the values previously published. Figure 2 shows spectra from the prostate phantom using the endorectal probe. The spectra are from a voxel size of 0.25 cc and show an even distribution of the metabolites (Cho 3.03ppm, Cr 3.93 & 3.22ppn, Cit 2.58pm) with some lipid contamination in the bottom row.

Conclusion:

A test-bed for the validation of prostate imaging and spectroscopic acquisition techniques is highly desirable. Such a test-bed can also be used for training purposes by either radiologists or radiation oncologists. The phantom is amenable to imaging by multiple modalities including ultrasound. It allows for testing deformation algorithms and also allows clinicians to practice image guided biopsy or brachytherapy procedures. While we have successfully tested this first prototype, additional work is necessary to further improve the stability of the phantom which would also include other anatomical structures.

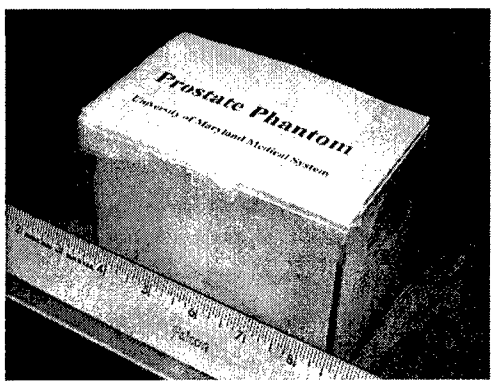

Figure 1: Prostate phantom.

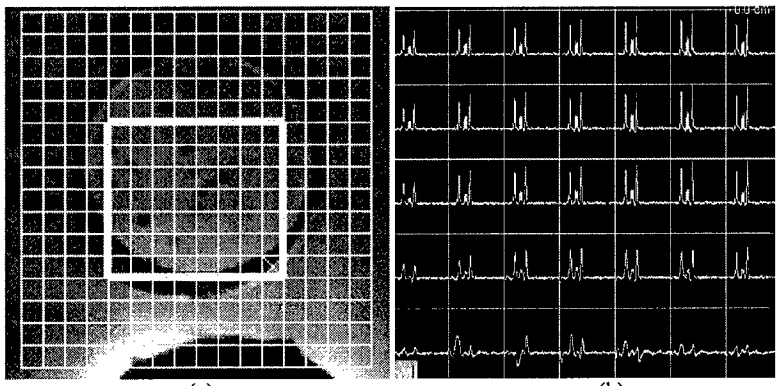

(a) (b)

Figure 2: (a) The MRS image and (b) the spectra of the prostate phantom.

References

Hamhaber U, et al., MRM 49:71-77, 2003.
Kemper J, Rofo. 2004 Aug;176(8):1094-9
Kurhanewicz J, et al., Radiol Clin North Am 2000;38:115-138.
Mizowaki T, et al., Int. J. Radiation Oncology Biol. Vol. 54, No. 5, pp1558-64, 2002.

APPENDIX B

MULTI-PURPOSE PROSTATE PHANTOM

Bao Zhang, Rao P. Gullapalli

Diagnostic Radiology Department, University of Maryland Medical Center, Baltimore, MD, United States

INTRODUCTION

Magnetic resonance imaging (MRI) and spectroscopy (MRS) along with the use of an endorectal coil has shown to increase the sensitivity and specificity in detecting prostate cancer (PCa) [Kurhanewicz 2000, Scheenen 2004]. However, its widespread use is limited by the complexity of such an exam. Often the clinicians and technologists are faced with learning the technique on a patient which is very limiting. Further the utility of this exam is to be able to accurately translate the findings to various treatment regimens such as brachytherapy. We have developed a prostate phantom that is compatible with most imaging modalities used for the diagnosis of prostate cancer. The phantom allows one to optimize pulse sequences, practice MRI and MRSI imaging techniques, practice either ultrasound or MRI guided prostate biopsy and can be used as a training tool for the placement of radioactive seeds.

MATERIALS

Agarose (Sigma Chemical Co., type I, Low EEO, EC No. 2327318);
Biochemicals: Choline, creatine, citrate;
Contrast agent: Gd-DTPA.

METHODS

Phantom Construction

In constructing the prostate phantom the T1 and T2 values of the prostate were given primary consideration followed by the Young's modulus of the prostate tissue from previously reported studies [Kemper 2004; Hamhaber 2003]. The prostate was constructed in an ellipsoid shape of dimensions 50x40x30 mm3 using 0.5% agarose gels 0.5% agarose gels doped with 0.1mM Gd-DTPA. Appropriate concentrations of biochemicals choline (10mM), creatine (30mM), citrate (100mM) and lactate (35 mM) that are predominantly seen in prostate MRSI were mixed with the agarose gel [Scheenen 2004]. To mimic implanted seeds, we used sesame seeds that were randomly distributed within the prostate. Lard was used to mimic the periprostatic fat and formed the outer layer of the entire prostate. Rubber tubing was used to mimic the urethra and the seminal vesicles. Plastic strips were positioned above the prostate to mimic the pubic arch. The phantom as shown in Fig. 1 allows for insertion of the endorectal coil or an ultrasound transducer through a rectangular tunnel and allows for the inflation of the balloon of the endorectal coil. There is a thin layer of deformable rubber between the tunnel and the prostate above. The rubber allows for the deformation to the prostate phantom and permits needle insertion for biopsy.

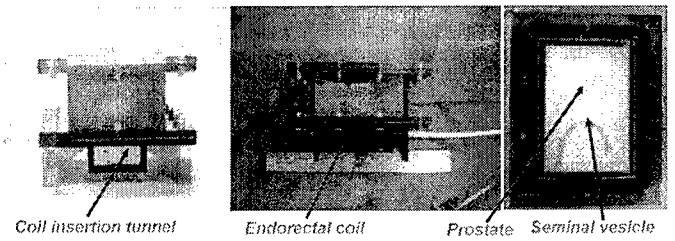

Fig. 1: The prostate phantom (left, middle) and its cross-sectional picture (right).

The detailed structure of the prostate phantom is shown in Fig. 2.

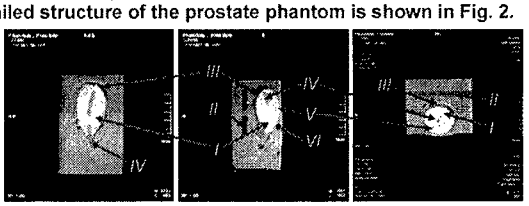

Fig. 2: MR prostate images in coronal (left), sagittal (middle) and transverse (right) planes. The arrows in the middle image point out I) prostate, II) pubis, III) fat, IV) urethra, V) seeds, and VI) seminal vesicle.

Imaging

The phantom was imaged on both Philips Eclipse 1.5T and Siemens 1.5T Avanto system and spectra were obtained using a PRESS CSI sequence (TE/TR=130/1500ms) with frequency selective fat and water suppression. T1 information on the phantom was obtained using inversion recovery sequences at various inversion times. T2 information on the phantom was obtained using a CPMG pulse with 32 echoes. The phantom was imaged over a 6 month period to check for stability.

RESULTS

The T1 value of the prostate phantom, periprostatic fat, and the agarose gel was 589±100 ms, 148 ±20 ms, and 1880±300 ms respectively. No significant changes were seen in the T1 values over the six month period. The T2 values of the prostate, periprostatic fat, and the agarose gel was 75±10 ms, 53±10 ms, and 90±15 ms respectively. These values dropped gradually by about 20% for all the three components over the six months. Over the six month period the chemical shift of Creatine changed by 0.18ppm, Cho by 0.18ppm, and citrate by 0.13ppm.

Figure 3 shows MRSI information from the prostate phantom taken six months apart. The spectra are well resolved at both the time points and show distinct peaks of choline, creatine (including the peak at 3.9ppm), and citrate.

The clinically relevant ratios of choline + creatine to citrate changed from 0.73 to 0.69 respectively. These results suggest that the phantom remains quite stable over long periods of time with appropriate storage.

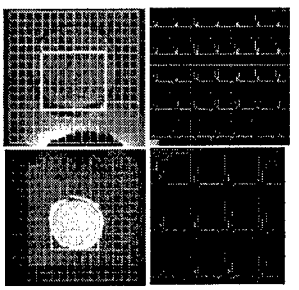

Fig. 3: The MRS images (left) and its spectra (right).

Figure 4 shows the color map of the choline+creatine to citrate ratio depicting a very uniform distribution of the metabolites is seen.
Figure 5 demonstrates the utility of the phantom using other imaging modalities. Here we demonstrate the images from the phantom using an ultrasound probe. The prostate phantom along with the inclusions (sesame seeds) are clearly visible in the phantom.

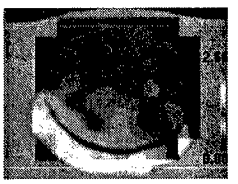

Fig. 4: The color map of the ratio Cho+Cr/Ci.

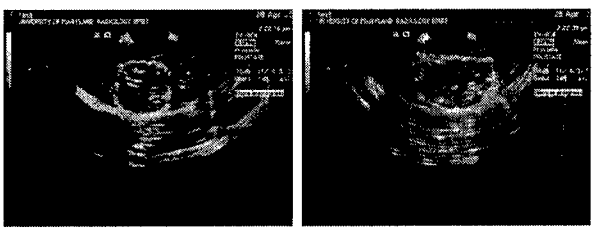

Fig. 5: The ultrasound images of the prostate phantom.

DISCUSSIONS AND CONCLUSIONS

We have developed a phantom that serves multiple uses. The phantom closely mimics the biochemical and the relaxation properties of the tissue. The main use of the phantom we envisage is for physician and technologists training and for quality control purposes especially for multi-center clinical trials. The phantom allows for the physician and technologist training so they may optimally image the patient rather than practice on the patient. Further it allows the physicians to train for fine needle biopsy or for placement of radioactive seeds under image guidance, using any of the imaging modalities. Added benefits of the phantom include testing of novel pulse sequence especially in the area of MRS, and for testing the quantitative efficacy of spectroscopic processing algorithms. Further, because the phantom can be imaged using various imaging modalities and with different size probes, it allows one to test registration algorithms across modalities and even prostate deformation correction algorithms within the same modality. While we have shown that the present version of the phantom is quite stable over a six month period, further work is underway to improve the stability of the phantom and various materials are being investigated to enable one to store the phantom at room temperature.

REFERENCES

Kurhanewicz J, et al. Radiol Clin North Am 2000;38:115-118
Hamhaber U, et al., MRM 49:71-77, 2003.
Kemper J, Rofo. 2004 Aug;176(8):1094-9.
Scheenen T., MRM 52:80-88, 2004.

APPENDIX C

Internal Report

Multimodality prostate image registration by 3D elastic deformation transformation

Bao Zhang, Rao P. Gullapalli
Department of Radiology
University of Maryland, Baltimore

ABSTRACT

A landmark-based non-rigid image registration procedure was developed and applied to the prostate images. The procedure consists of 2 steps. The first step is to pick up the landmarks (points, curves or surfaces) manually. Then the pixel/voxel correspondences between the source and target images are established. In the second step, the images are registered by the novel registration algorithm, which is based on the theory of strain energy minimization. The registration of the source and target images comply with the correspondences generated in first step. This algorithm was tested on synthetic, phantom and real prostate images. The registration results demonstrate that the volume of interest can be properly deformed.

INTRODUCTION

Endorectal coil procedure has become a standard procedure in prostate imaging. However, this procedure experiences dramatic prostate deformation because of the inflation of the coil balloon. Image registration is thus needed in prostate surgery to guide the treatment plan following deformation correction.

Image registration is a procedure of determining a one-to-one transformation between 2 image spaces which maps each pixel/voxel in one image onto the corresponding pixel/voxel in another image. The transformation may be classified into 2 categories: rigid and non-rigid transformation. Rigid transformation can deal with translation and rotation, which describes the global deformation of the image. Non-rigid, or elastic transformation, on the other hand, deals with the local deformation. There are two major physical models upon which the elastic transformation is based: elastic model and fluid model.[1] In the elastic model, force balance equations are used to determine the deformation; and in the fluid model, principles of fluid dynamics are used.

The algorithm we proposed here falls in the elastic category which is based on the strain energy minimization of an elastic volume. It only focuses on the strain energy of the elastic volume while ignoring the complex internal forces.[2] The algorithm simplifies the registration problem dramatically.

MATERIALS AND METHODS

Energy minimization theory

According the principles in dynamics, the strain energy of an elastic volume has a stationary value in its steady state. That is, $\delta U = 0$. This equation holds whether or not the volume of interest is in a free or stressed state.

Strain energy

Given a general state of stress, the strain energy density U_0 (strain energy per volume) of an elastic volume is:

$$U_0 = \frac{1}{2}\left[\lambda e^2 + 2G(\varepsilon_x^2 + \varepsilon_y^2 + \varepsilon_z^2) + G(\gamma_{xy}^2 + \gamma_{yz}^2 + \gamma_{xz}^2)\right]$$

where, λ and G are Lame constants characterizing material mechanical properties, ε_p ($p = x, y$ or z) is the normal strain in p direction, γ_{pq} ($pq = xy, yz$ or xz) is the shear strain in a plane normal to p direction pointing to q direction, e is the unit volume change. For incompressible materials, e is zero. Thus the strain energy density is simplified as:

$$U_0 = G(\varepsilon_x^2 + \varepsilon_y^2 + \varepsilon_z^2) + \frac{1}{2}G(\gamma_{xy}^2 + \gamma_{yz}^2 + \gamma_{xz}^2)$$

So the strain energy U of an elastic body V is:

$$U = \iiint_V U_0 dV$$

$$= G\iiint_V \left[(\varepsilon_x^2 + \varepsilon_y^2 + \varepsilon_z^2) + \frac{1}{2}(\gamma_{xy}^2 + \gamma_{yz}^2 + \gamma_{xz}^2)\right] dV$$

According to the strain-displacement relationship:

$$\varepsilon_x = \frac{\partial u}{\partial x} \qquad \varepsilon_y = \frac{\partial v}{\partial y} \qquad \varepsilon_z = \frac{\partial w}{\partial z}$$

$$\gamma_{xy} = \frac{\partial u}{\partial y} + \frac{\partial v}{\partial x} \qquad \gamma_{yz} = \frac{\partial v}{\partial z} + \frac{\partial w}{\partial y} \qquad \gamma_{xz} = \frac{\partial u}{\partial z} + \frac{\partial w}{\partial x}$$

where u,v, and w are the displacements in x, y and z direction, respectively, the strain energy is rewritten as:

$$U = G\iiint\left[\left(\frac{\partial u}{\partial x}\right)^2 + \left(\frac{\partial v}{\partial y}\right)^2 + \left(\frac{\partial w}{\partial z}\right)^2\right]dxdydz + \frac{1}{2}G\iiint\left[\left(\frac{\partial u}{\partial y} + \frac{\partial v}{\partial x}\right)^2 + \left(\frac{\partial v}{\partial z} + \frac{\partial w}{\partial y}\right)^2 + \left(\frac{\partial u}{\partial z} + \frac{\partial w}{\partial x}\right)^2\right]dxdydz$$

Eq 1.

This energy minimization theory is applied to elastic image registration. Suppose we have 2 image volumes V1 and V2. V1 is the volume before deformation, and V2 is the volume after deformation. The voxel position in V1, which is denoted as (x_{ijk}, y_{ijk}, z_{ijk}), evolves into position (X_{ijk}, Y_{ijk}, Z_{ijk}) in V2. Taken V1 as the reference and using the forward difference formula for first derivative, the solutions for Equation 1 are derived, in discrete form, as follows:

$$X_{ijk} = \frac{\left[\begin{array}{l} 2X_{i+1jk} + 2X_{i-1jk} + X_{ij+1k} + X_{ij-1k} + X_{ijk+1} + X_{ijk-1} + (Y_{i+1jk} - Y_{ijk}) - \\ (Y_{i+1j-1k} - Y_{ij-1k}) + (Z_{i+1jk} - Z_{ijk}) - (Z_{i+1jk-1} - Z_{ijk-1}) \end{array}\right]}{8}$$

$$Y_{ijk} = \frac{\left[\begin{array}{l} Y_{i+1jk} + Y_{i-1jk} + 2Y_{ij+1k} + 2Y_{ij-1k} + Y_{ijk+1} + Y_{ijk-1} + (Z_{ij+1k} - Z_{ijk}) - \\ (Z_{ij+1k-1} - Z_{ijk-1}) + (X_{ij+1k} - X_{ijk}) - (X_{i-1j+1k} - {}_{i-1jk}) \end{array}\right]}{8}$$

$$Z_{ijk} = \frac{\left[\begin{array}{l} Z_{i+1jk} + Z_{i-1jk} + Z_{ij+1k} + Z_{ij-1k} + 2Z_{ijk+1} + 2Z_{ijk-1} + (X_{ijk+1} - X_{ijk}) - \\ (X_{i-1jk+1} - X_{i-1jk}) + (Y_{ijk+1} - Y_{ijk}) - (Y_{ij-1k+1} - Y_{ij-1k}) \end{array}\right]}{8}$$

For plane strain, without the loss of generality, we assume that all z components of the strain are zero. That is, $\varepsilon_z = \gamma_{xz} = \gamma_{yz} = 0$. Thus the preceding solutions are simplified as:

$$X_{ij} = \frac{2X_{i+1j} + 2X_{i-1j} + X_{ij+1} + X_{ij-1} + (Y_{i+1j} - Y_{ij}) - (Y_{i+1j-1} - Y_{ij-1})}{6}$$

$$Y_{ij} = \frac{Y_{i+1j} + Y_{i-1j} + 2Y_{ij+1} + 2Y_{ij-1} + (X_{ij+1} - X_{ij}) - (X_{i-1j+1} - X_{i-1j})}{6}$$

The solutions may be applied to 2-dimensional image registration.

The solutions may be further simplified by ignoring the shear strain ($\gamma_{xy} = 0$) as:

$$X_{ij} = \frac{X_{i+1j} + X_{i-1j}}{2}$$

$$Y_{ij} = \frac{Y_{ij+1} + Y_{ij-1}}{2}$$

In this solution, there is no coupling between positions in X and Y directions. Either one of the solutions can be applied to the registration of an elastic string (1-dimension).

RESULTS

This novel registration algorithm was tested on numerical simulation first, then on prostate phantom, and finally was applied to real prostate images. The results are depicted below.

1. *Numerical simulation*

In the numerical simulation, a sphere (radius, 10) is elastically deformed to an ellipsoid (the three semiaxes: a=9, b=12, c=10). Both the sphere and the ellipsoid are located at the center of a 30X30X30 cubic pixels volume. Fig. 1 displays the geometric shapes of the sphere and the ellipsoid. A portion of the MR prostate volume is synthesized in the sphere and the ellipsoid, respectively.

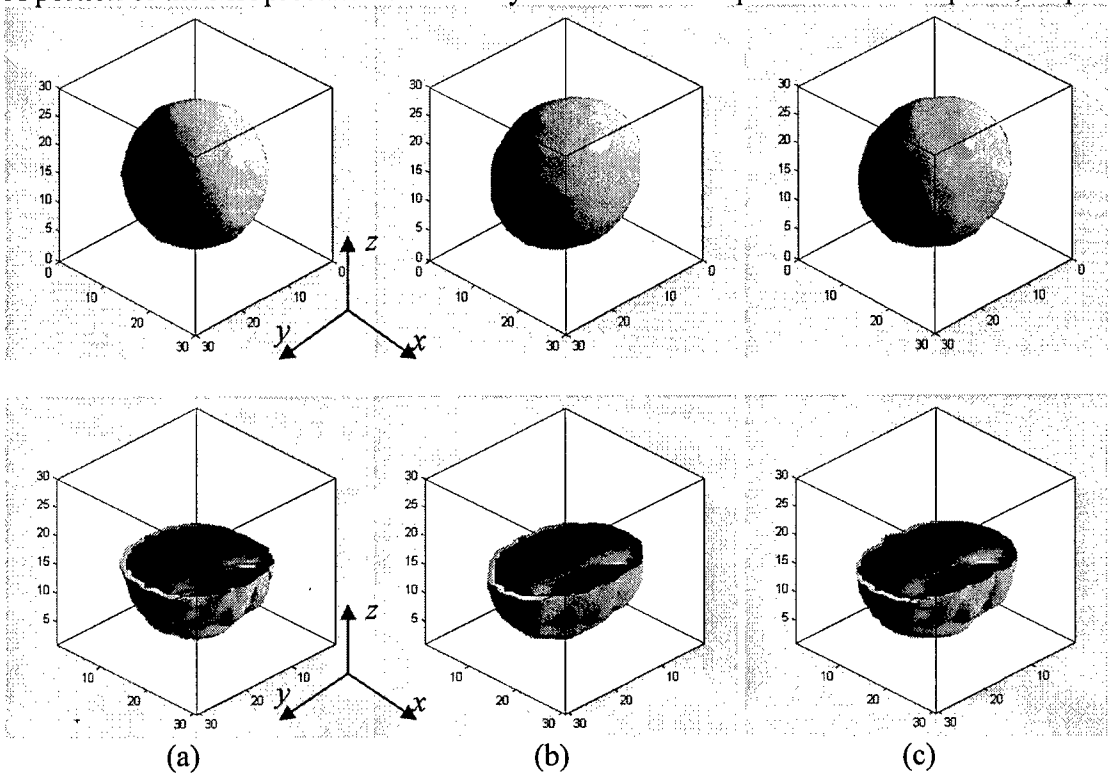

Fig. 1: The 3D geometric shape of (a) the source sphere, (b) the target ellipsoid, and (c) the registered result from source to target.

As shown in Fig. 1, the surfaces of the source and the target serve as the constraints of the elastic deformation. Taking the correspondent surfaces as the input of our registration algorithm, the result is shown as Fig. 1c.

Fig. 2 depicts the registration results in three orthogonal planes, xy plane, yz plane, and xz plane. The displacement distributions along the three orthogonal planes are displayed in Fig. 3 as well.

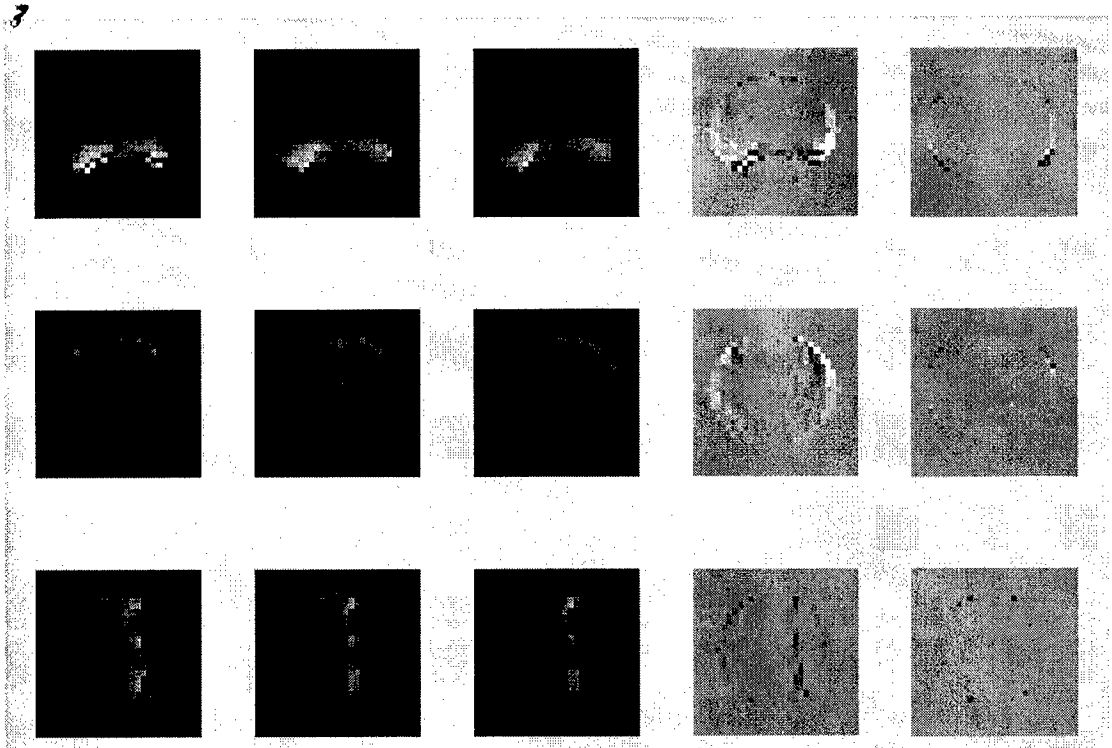

Fig. 2: the registration results of three orthogonal planes. First row lists the resulting 2D images of xy plane; second row, yz plane; third row, xz plane. The first column are the central images of the source sphere; the second column, target ellipsoid; the third, registered image from source to target; the fourth, difference between the source and target images; and fifth, difference between the target and the registered images.

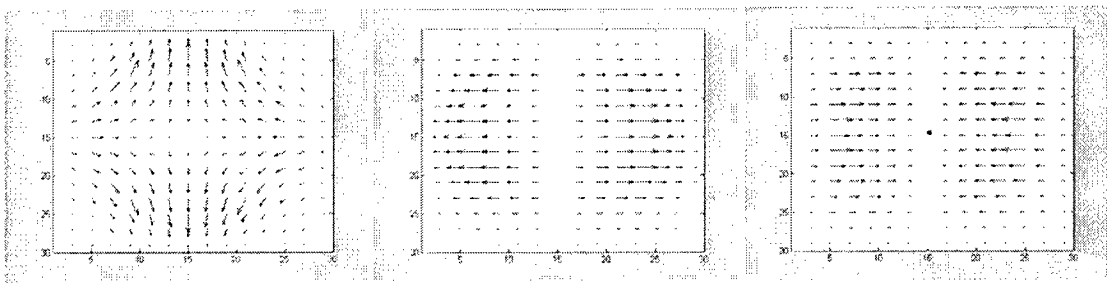

(a) (b) (c)

Fig. 3: the displacement distribution in (a) xy plane, (b) yz plane, and (c)xz plane.

2. *Prostate phantom*

In this section, the registration results on the prostate phantom are displayed. Fig. 4 shows the image registration in the axial image plane. Figure 4a shows the source image, i.e., the image obtained with the use of the endorectal coil at full inflation. Figure 4b is the target image that was obtained with the endorectal coil deflated and figure 4c shows the correction made to the source image. The sesame seeds within the prostate phantom serve as landmarks and are an indication of the quality of the elastic registration.

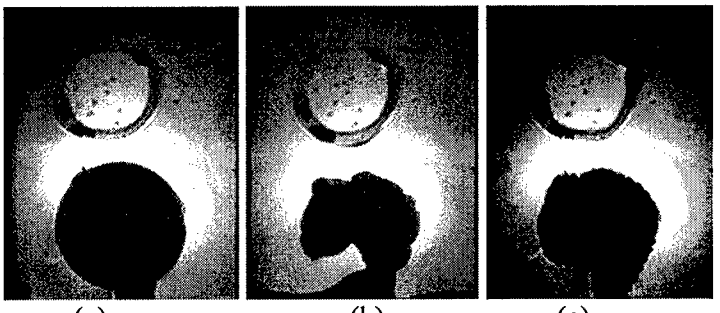

(a) (b) (c)

Fig. 4: a) source, b) target, and c) registered volumes. The dark spots shown in the top surfaces of the volumes on the second are sesame seeds randomly distributed in the phantom to validate our registration algorithm.

Figure 5 shows the displacement distribution along the 3 orthogonal central planes for the same slices as shown in Figure 4

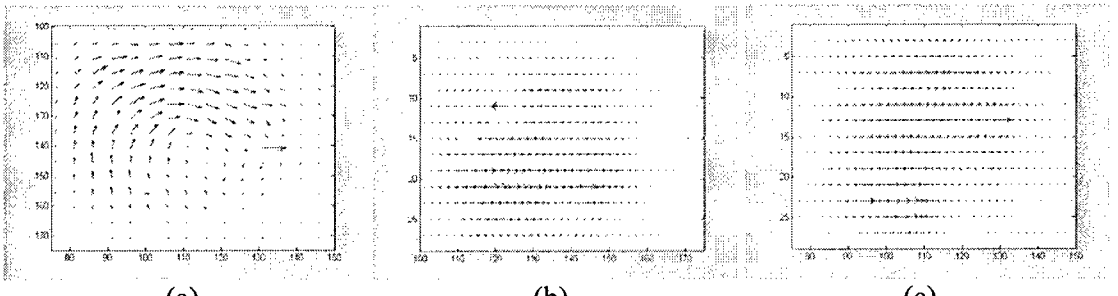

(a) (b) (c)

Fig. 5: the displacement distribution in (a) xy plane, (b) yz plane, and (c)xz plane.

3. *In Vivo Prostate Data*

The results on the real prostate data are displayed in this section. Figure 6a shows an image of the prostate obtained using the endorectal coil at full inflation. Figure 6b is the image of the same prostate obtained without any inflation of the balloon. Figure 6c is the result of our deformation correction and registration of the image shown in Fig. 6b to the target image shown in Fig 6a. Note the similarities between the images shown in Figures 6a and 6c. Please note the deformation correction and registration can be applied for cases where the deformed object needs to be corrected or vice-versa.

(a) (b) (c)

Fig. 6: the prostate images in the axial image plane. a) deformed, b) normal, and c) registered.

Conclusions

Our initial results indicate that the strain energy minimization technique for elastic registration works well for deformable objects such as the prostate. Further studies need to be performed to quantify the accuracies achievable with this technique using the prostate phantom.

References:

1. Miller MI, Christensen GE, Amit Y, and Gerander U, Mathematical textbook of deformable neuroanatomies, Proc Natl Acad Sc,90:11944-48, 1993.
2. Rohr K, Stiehl S, Sprengel R, Buzug TM, Wesse J and Kahn MH, Landmark based elastic registration using approximating thin-plate splines, IEEE Trans Med Imag. 20:526-534, 2001.